JOURNAL OF Materials CHEMISTRY

The crystal and electronic structure analysis of $(OMTTF)_2[Ni(tdas)_2]$†

Hideki Yamochi,*[a,b] Norihito Sogoshi,[a] Yasuhiro Simizu,[a] Gunzi Saito*[a] and Kiyoshi Matsumoto[c]

[a]*Division of Chemistry, Graduate School of Science, Kyoto University, Sakyo-ku, Kyoto 606-8502, Japan. E-mail: yamochi@kuchem.kyoto-u.ac.jp*
[b]*CREST, Japan Science and Technology Corporation (JST), Japan*
[c]*Graduate School of Human and Environment Studies, Kyoto University, Sakyo-ku, Kyoto 606-8501, Japan*

Received 1st February 2001, Accepted 14th May 2001
First published as an Advance Article on the web 6th June 2001

The crystal structure of $(OMTTF)_2[Ni(tdas)_2]$ (OMTTF = octamethylenetetrathiafulvalene and tdas = 1,2,5-thiadiazole-3,4-dithiolate) was solved as the second example of an $M(tdas)_2$ (M = transition metal) complex with TTF derivatives. The structure consists of a dimer of the radical cation of the OMTTF molecules and the $Ni(tdas)_2$ dianion, which are located in the cation and anion sites in an NaCl-type structure, respectively. The degree of charge-transfer (CT) is determined from optical spectra, which are interpreted as the superposition of those of radical cation and the dianion. Although the atomic orbital (AO) coefficients of the terminal sulfur atoms of $[Ni(tdas)_2]$ are significantly large in the HOMO of the dianion, the packing motif of this complex prohibited the formation of a three-dimensional network of intermolecular interactions. Also, a peculiarity of the energy diagram of the molecular orbitals (MO) of tdas is discussed on the basis of semiempirical MO calculations.

Introduction

Underhill and co-worker synthesized the chemical species $[M(tdas)_2]^{n-}$, where M = Ni, Pd, Pt, and Cu ($n = 2$), and M = Fe ($n = 1$) in 1990 (for chemical structures, see Scheme 1).[1] Subsequently, crystal structures were reported for the tetraalkylammonium and tetrabutylphosphonium complexes of $Ni(tdas)_2$ and $Fe(tdas)_2$.[2] It is noteworthy that $(Bu_4N)[Fe(tdas)_2]$ showed a peculiar phase transition with reentrant magnetism.[2c]

As for the application of this series of metal–dithiolene ligands (DTL) to conductive molecular crystals, $(TTF)_2[Ni(tdas)_2]$ is reported to show relatively high conductivity at room temperature (σ_{rt}) of 0.1 S cm^{-1}.[1] However, structural information on $M(tdas)_2$ complexes with TTF and its derivatives has been rarely reported. Only the crystal structure of $(TTF)_2[Fe(tdas)_2]$, which is less conductive than the $Ni(tdas)_2$ complex, has been presented and shown to be a layered structure.[3] The chemical structures of $M(tdas)_2$ show the sulfur atoms to be at the terminal positions along the molecular longitudinal axis, from which one can expect the occurrence of three-dimensional intermolecular interactions. In connection with the interlayer interactions in the two-dimensional organic superconductors of BEDT-TTF complexes,[4] we have examined the complex formation of $Ni(tdas)_2$ with typical donor molecules of TTF derivatives. This paper describes electronic and structural aspects of the title complex, which shows a completely different packing pattern to that of $(TTF)_2[Fe(tdas)_2]$, along with a comparison of tdas with other DTLs based on semiempirical MO calculations.

Experimental

$(Bu_4N)_2[Ni(tdas)_2]$ was prepared according to the reported procedures.[1] The product recrystallized from a mixture of ethanol and water and then from ethanol gave a satisfactory elemental analysis (C, H, N within 0.3%). The complex formations were carried out by the electrocrystallization method in the presence of $(Bu_4N)_2[Ni(tdas)_2]$ in 1,1,2-trichloroethane, CH_3CN, or tetrahydrofuran. The donor molecules OMTTF, TMTTF, BEDO-TTF, and TMTSF afforded solid products, while TTF, TTC_1-TTF, and BEDT-TTF did not. Among the former products, only the OMTTF complex was of adequate quality for single crystal X-ray structure analysis. Also, it should be noted that the yield of the complexes was extremely poor in general and the compositions could not be determined, except for in the case of $(OMTTF)_2[Ni(tdas)_2]$ as briefly reported previously.[5] Hereafter, this paper will concentrate only on this complex.

The typical conditions for the complex preparation were as follows. In an H-shaped glass cell, which has a glass filter to separate the anodic and cathodic chambers, 4.3 mg of OMTTF and 94.2 mg of $(Bu_4N)_2[Ni(tdas)_2]$ were dissolved in 18 mL of

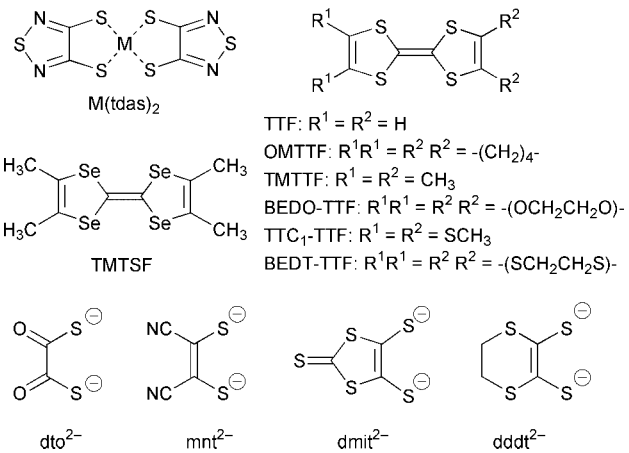

Scheme 1 Chemical structures of the compounds discussed in the text.

†OMTTF = octamethylenetetrathiafulvalene and tdas = 1,2,5-thiadiazole-3,4-dithiolate.

 DOI: 10.1039/b101909k

acetonitrile. A constant current of 2 μA was applied for 140 days to afford 5.8 mg of shiny black plates.

The intensity data of the structural analysis were collected on an automatic four circle diffractometer with monochromated MoKα radiation at room temperature. The structure was solved by direct methods using Crystan GM6.3.[6] The refinements were performed by the full-matrix, least-squares method. Cyclic voltammetry (CV) was carried out in a 0.1 M solution of $Bu_4N{\cdot}BF_4$ in CH_3CN with Pt electrodes *vs.* SCE at a scan rate of $100\ mV\ s^{-1}$ using a Yanaco Polarographic Analyzer P-1100 at room temperature. Optical measurements were carried out for KBr disks on a Perkin-Elmer 1600 Series spectrometer in the IR region (400–7800 cm^{-1}) and on a Shimadzu UV-3100 spectrometer for near-infrared, visible and ultraviolet (UV–VIS–NIR) regions (3800–42000 cm^{-1}). The EPR spectra were recorded with a JEOL JES-RE2X X-band EPR spectrometer. The spectra recorded as the first derivative signals were integrated numerically to give the absorption spectra. To calculate the spin susceptibility of the sample, the area intensity of the latter was compared with that of $CuSO_4{\cdot}5H_2O$ derived by the same method.

The extended Hückel method was employed to calculate the molecular orbitals (MOs) and the intermolecular overlap integrals based on the molecular geometry obtained by crystal structure analysis.[7] To compare the MOs of the ligands, the geometry optimization and MO calculations were carried out by the semiempirical method, MOPAC97, applying the AM1 Hamiltonian.[8]

Results and discussion

Structural and physical aspects of $(OMTTF)_2[Ni(tdas)_2]$

The room temperature conductivity of $(OMTTF)_2[Ni(tdas)_2]$ measured on a compressed powder by the conventional two probe method is $3.7\times10^{-9}\ S\ cm^{-1}$.[9] The optical spectra dispersed in KBr (Fig. 1) above $5\times10^3\ cm^{-1}$ are well described as the superposition of intramolecular transitions of $OMTTF^{+\bullet}$ at 17.2 and $24.0\times10^3\ cm^{-1}$ and $[Ni(tdas)_2]^{2-}$ at 20.5 and $31.5\times10^3\ cm^{-1}$. The band at $11.3\times10^3\ cm^{-1}$ is assigned to the intermolecular transition between the OMTTF radical cations by comparison to those of (OMTTF)Br and $(OMTTF)_2[M(dto)_2]$.[10] A characteristic band ascribed to the electronic transitions between the partially oxidized species, which should be found below $5\times10^3\ cm^{-1}$, is absent. Also, the vibrational absorption bands assigned to the a_g modes of $OMTTF^{+\bullet}$, by analogy with those of $TMTTF^{+\bullet}$,[10] are observed, indicating the existence of the donor dimer in an isolated position or in a segregated column. These results indicate that this complex is completely ionized.

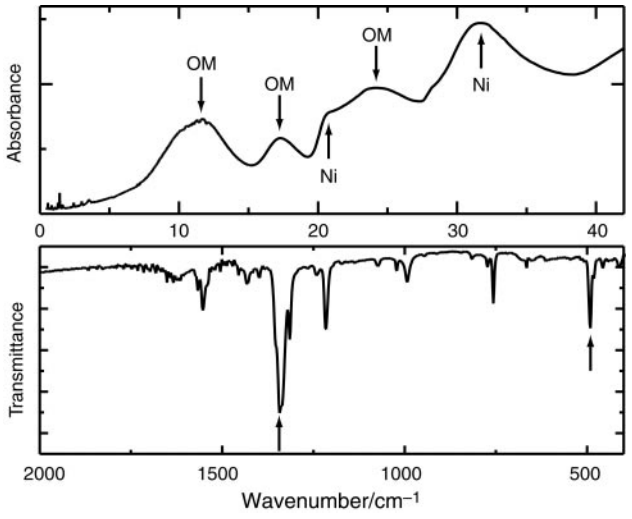

Fig. 1 Optical spectra of $(OMTTF)_2[Ni(tdas)_2]$ dispersed in KBr. The absorption bands in the electronic transition region (top) are assigned to those from $OMTTF^{+\bullet}$ (11.3, 17.2, $24.0\times10^3\ cm^{-1}$) and $[Ni(tdas)_2]^{2-}$ (20.5, $31.5\times10^3\ cm^{-1}$) indicated as OM and Ni, respectively. In the vibrational region, the a_g mode transitions of the dimer of $OMTTF^{+\bullet}$ are observed at 1347 and 496 cm^{-1} as indicated by the arrows in the bottom panel.

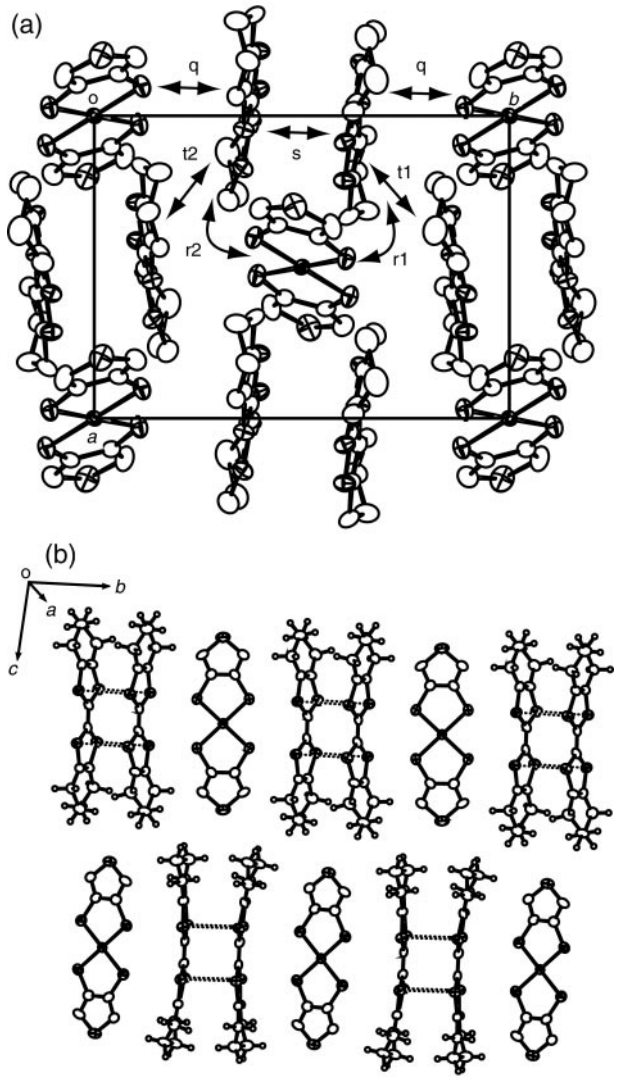

Fig. 2 The crystal structure of $(OMTTF)_2[Ni(tdas)_2]$. (a) Projection along the *c*-axis. The hydrogen atoms are omitted for simplicity. The values of the intermolecular overlap integrals are $s=47.4$, $t_1\approx t_2\approx0.01$, $q=0.2$, $r_1=1.5$, $r_2=1.6\times10^{-3}$. (b) Projection of the molecules on the (201) plane projected on to the molecular plane of $Ni(tdas)_2$. The top and bottom rows are located at $x=0.5$ and $x=1.0$, respectively. The dotted lines indicate intermolecular S···S contacts shorter than 3.60 Å.

The crystal structure‡ of $(OMTTF)_2[Ni(tdas)_2]$ consists of a dimer of the donor radical cations and the $Ni(tdas)_2$ dianion (Fig. 2).[11] In the donor dimer, the crystallographically parallel OMTTF molecules, which are related to each other by a center of inversion, show a nearly superimposed overlap pattern with an interplanar distance of 3.53 Å. The molecular plane of the dianion is nearly perpendicular to that of OMTTF (dihedral angle = 85.4°). $[Ni(tdas)_2]^{2-}$ shows a planar molecular structure with a maximum deviation of the constituent atom of 0.06 Å from the best plane. The bond lengths are identical to those in the reported tetraalkylammonium salts[2b] within the estimated standard deviations. Intermolecular heteroatom contacts shorter than the sum of the van der Waals radii (vdW) are

†CCDC reference number 159339. See http://www.rsc.org/suppdata/jm/b1/b101909k/ for crystallographic files in .cif or other electronic format.

observed only within the donor dimer with distances of 3.403(3)–3.432(3) Å. The structure of this complex is best expressed as an NaCl-type packing, in which an OMTTF dimer is surrounded by six $Ni(tdas)_2$ in a three-dimensional fashion and *vice versa*.

The packing pattern of $(OMTTF)_2[Ni(tdas)_2]$ resembles those of $(ET)_2[Ni(dto)_2]$ and α-$(ET)_2[Pd(dto)_2]$ in which NaCl-type structures are also formed by the fully ionized dimer of the donor radical cation and dianion of the metal–ligand systems, respectively.[10] A difference between these complexes, however, appeared in the relative arrangement of the donor and the dianion along the molecular longitudinal axis. While the longitudinal axis of the $Ni(tdas)_2$ dianion passes through the intermediate position between the molecules in the neighboring donor dimer, that of $M(dto)_2$ [M = Ni, Pd (α)] pierces a donor molecule in the dimer (Fig. 3). The terminus of $M(dto)_2$ consists of oxygen atoms at the corners of the rectangular molecule and hence has a bay region which can accommodate the terminal hydrogen atoms of the donor molecule. On the other hand, $Ni(tdas)_2$ possesses a terminal sulfur atom on the longitudinal axis. Without the specific intermolecular interactions such as heteroatom contacts, which increase the electronic stabilization, or hydrogen bonds with acidic hydrogen atoms, it is natural to avoid intermolecular short atomic contacts when the component molecules construct a crystal structure. The difference in the packing patterns between $Ni(tdas)_2$ and $M(dto)_2$ complexes may come from the molecular shape of the dianions, the termini of which can penetrate into the hollow site of the donor dimer and accommodate the terminal part of a donor molecule, respectively.

Although it is a phenomenological feature based on a small number of examples, it should be noted that the dimerized packing of $M(tdas)_2$ with a deformed molecular structure has been observed only in complexes that contain the monoanions of this metal–ligand system.[2,3]

The intermolecular overlap integrals calculated by the extended Hückel method showed strong dimerization of the OMTTF, for which the overlap integral is more than *ca.* 30 times bigger than the others. The LUMO of $Ni(tdas)_2$, which is the HOMO of the dianion, shows the biggest AO coefficients at the terminal sulfur atoms as shown in Fig. 4. Hence, intermolecular interactions along the molecular longitudinal axis are expected. However, along the longitudinal axis of $Ni(tdas)_2$, the OMTTF dimers are located in the best plane of the dianion as mentioned before. Since the terminal parts

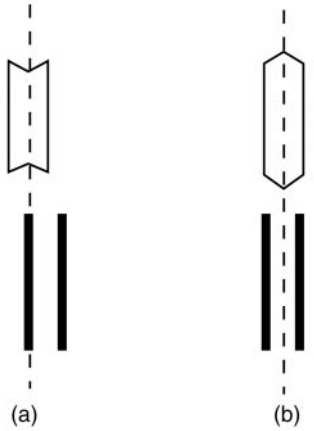

Fig. 3 Schematic representation of the relative orientations of the donor dimer and the metal–ligand system in (a) $(ET)_2[M(dto)_2]$ and (b) $(OMTTF)_2[Ni(tdas)_2]$ complexes. The open rectangular-like hexagon, thick line, and dashed line indicate the top-view of the metal–ligand system, the side-view of the donor molecule, and the longitudinal axis of the former, respectively.

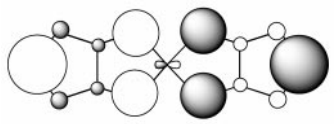

Fig. 4 Schematic representation of the LUMO of $Ni(tdas)_2$ (HOMO of $[Ni(tdas)_2]^{2-}$) calculated by the extended Hückel method based on the molecular structure in $(OMTTF)_2[Ni(tdas)_2]$. The absolute values of the coefficients are 0.47, 0.10, 0.14, 0.36, and 0.12 for the p_z AOs of the terminal sulfur, nitrogen, carbon, inner sulfur atoms and for the d_{xz} AO of Ni, respectively.

of the donor molecules are covered by the alkyl groups, the intermolecular overlap integral was negligible along this direction.

Consistent with these structural and optical features, the intensity of the EPR signal observed at room temperature gave a spin susceptibility (χ_s) of 9×10^{-6} emu per formula unit, which corresponded to a spin concentration of 0.7% per formula unit, assuming the Curie law.[12] It is most plausible that the spins on the donor molecules are strongly coupled within a dimer and the observed signal is ascribed to a defect of the crystal.

All of the results of the optical, structural, and magnetic measurements revealed that $Ni(tdas)_2$ provides an isolated π-electron system in the OMTTF complex despite the peculiar feature of the LUMO which has the biggest AO coefficients at the terminal sulfur atoms.

Redox properties of the $M(DTL)_2$ system

To discuss the electronic structure of $Ni(tdas)_2$, its redox properties were reexamined. Although it was reported that $[Ni(tdas)_2]^{2-}$ showed a quasi-reversible one-electron oxidation at +0.95 V *vs.* Ag/AgCl in CH_3CN,[1] we observed two-step redox processes in the same solvent at +0.18 (reversible) and +0.81 V (irreversible) *vs.* SCE for $[Ni(tdas)_2]^{2-} \rightleftarrows [Ni(tdas)_2]^{-\bullet}$, and $[Ni(tdas)_2]^{-\bullet} \rightleftarrows [Ni(tdas)_2]$, respectively.[13]

It should be mentioned that the degree of CT in the title complex is mostly explained by the criterion to realize the partial CT ground states in the 1:1 TTF–TCNQ system.[14] That is, representing the redox potentials of the donor and acceptor molecules under the same conditions of measurement by E_D and E_A, respectively, it is reported that the ionic, partial CT, and neutral ground states are preferred when $E_D - E_A$ is less than −0.02, between −0.02 and +0.34, and more than +0.34 V, respectively. For the combination of OMTTF and $Ni(tdas)_2$ this involves the four redox potentials E_D^1, E_D^2, E_A^1, and E_A^2, which correspond to the redox processes of $OMTTF \rightleftarrows (OMTTF)^{+\bullet}$ (0.29 V), $(OMTTF)^{+\bullet} \rightleftarrows (OMTTF)^{2+}$ (0.69 V), $Ni(tdas)_2 \rightleftarrows [Ni(tdas)_2]^{-\bullet}$ (0.81 V), and $[Ni(tdas)_2]^{-\bullet} \rightleftarrows [Ni(tdas)_2]^{2-}$ (0.18 V), respectively. Since $E_D^1 - E_A^1 < -0.02$ V, the donor and acceptor are ionized to $(OMTTF)^{+\bullet}$ and $[Ni(tdas)_2]^{-\bullet}$ in a complex. As far as further CT is concerned, the radical ion pair cannot give the divalent ion pair of $(OMTTF)^{2+}$ and $[Ni(tdas)_2]^{2-}$, since $E_D^2 - E_A^2 > 0.34$ V. The radical anion, however, can ionize another donor molecule due to the high redox potential of E_A^2. Although partial CT is expected between the second OMTTF and $[Ni(tdas)_2]^{-\bullet}$ from the value of $E_D^1 - E_A^2 = 0.11$ V, the observed results showed a completely ionized state for $(OMTTF^{+\bullet})_2[Ni(tdas)_2{}^{2-}]$ in the complex. This discrepancy may come from the limitation of the criteria when applied to systems other than 1:1 TTF–TCNQ. Also, since $E_D^2 - E_A^1 < -0.02$ V, this treatment allows us to expect the formation of the complex $(OMTTF^{2+})[Ni(tdas)_2{}^{-\bullet}]_2$, the preparation of which should be examined. It should be noted that the other donor molecules examined here also show first and second redox potentials, from which similar compositions and degrees of ionization to those of

Table 1 Comparison of the calculated LUMO energy and redox potentials of the ML_2 dianion

	LUMO energy/eV	Redox potential of $[ML_2]^{2-} \rightleftarrows [ML_2]^{-\bullet}$/V				
		cNi	M = Pd	M = Pt	M = Cu	Note
dto	0.776	+0.57	+1.33	+0.90	+0.12	[a]
mnt	1.139	+0.23	+0.46	+0.21	+0.34	[b]
dmit	0.564	−0.19	−0.09	−0.27	−0.07	[c]
dddt	1.183	−0.81	−0.43	−0.59	−0.49	[d]
tdas	0.631	+0.18	—	—	—	

[a]Oxidation peak potentials in CH_3CN *vs.* SCE (ref. 10). [b]In CH_3CN *vs.* SCE (ref. 15). [c]In CH_3CN *vs.* SCE (ref. 16). [d]In dimethylformamide *vs.* Ag/AgCl (ref. 17).

OMTTF are expected in their $Ni(tdas)_2$ complexes, according to the same treatment as above.

Although it is not yet clear why $Ni(tdas)_2$ afforded only a small number of CT complexes of extremely poor crystal quality in general, it is interesting to modify the redox properties of this chemical species to develop a wider variety of complexes in this family. As one of the methods of changing the redox potentials, substitution of the central transition metal will be effective. In fact, a drastic difference in the redox potentials has been observed in the $M(dto)_2$ system.[10] Let us compare the calculated MOs of tdas with those of the representative DTLs of dto, mnt, dmit, and dddt to estimate the variation of the redox potentials of $[M(tdas)_2]^{2-}$. The geometry optimization of each DTL in the dianionic state gave an almost planar geometry when an appropriate initial molecular shape was given. The orbital energies of the LUMOs (HOMOs of the dianions) are listed in Table 1 along with the observed redox potentials of the process $[M(DTL)_2]^{2-} \rightleftarrows [M(DTL)_2]^{-\bullet}$ (M = Ni, Pd, Pt, Cu). No clear correlation was observed between the calculated LUMO level of the DTL and the observed redox potential of $M(DTL)_2^{2-}$, even for the same M. These results indicate that the redox potential of an $M(DTL)_2$ is determined by the complicated combination of the MOs of M and DTL. It has been emphasized that the redox potentials of $M(dto)_2^{2-}$ are very sensitive to the central transition metal in comparison to other $M(DTL)_2$ systems.[10] In fact, the maximum difference in the redox potentials for $M(dto)_2$ is 1.21 V, while that of the other $M(DTL)_2$ species is 0.38 V at most. To understand these phenomena, Fig. 5 shows the calculated energy levels around the LUMO of each DTL. In all cases, the next LUMOs are located at more than 5.7 eV above the LUMOs in the diagram (not indicated in Fig. 5). The species dto and tdas show a narrow gap between the LUMO and HOMO compared to the other DTLs. The complicated and large dependence on M of the redox potential of $M(dto)_2^{2-}$ can be regarded as a result of this peculiarity, since not only the LUMO, but also the HOMO, of dto contributes to the energy level of the LUMO of $M(dto)_2$ when the energy levels of the ligand are close to that of M. The calculated results indicate that tdas is an interesting ligand in this regard and it is expected to show a huge dependence on M of the redox potentials of $M(tdas)_2^{2-}$, though only the synthesis and no redox properties have been reported for the metal–ligand systems of M = Pd, Pt, Cu, and Fe.

Concluding remarks

As is expected from the discussion above, the metal–ligand system of $M(tdas)_2$ is expected to show a variety of redox properties depending on M, and, hence, its CT complexes are of interest. However, only the semiconducting $(TTF)_2[Fe(tdas)_2]$ and the insulating $(OMTTF)[Ni(tdas)_2]$ are well defined complexes of TTF derivatives at present. Further synthetic efforts are needed to reveal the nature of the tdas ligand.

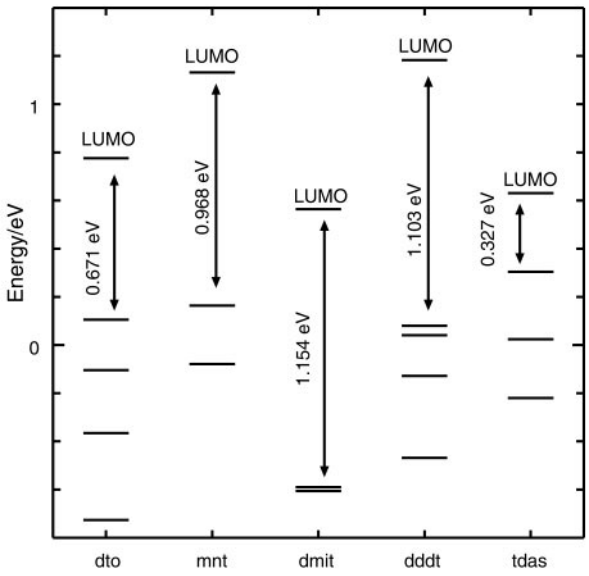

Fig. 5 Schematic representation of the MO levels around the LUMOs for DTLs calculated by MOPAC and based on the geometry-optimized conformations for the dianions.

Acknowledgements

It is with great pleasure that the authors would like to dedicate this article to the occasion of the retirement of Professor Underhill. This work was, in part, supported by a Grant-in-Aid for Scientific Research from the Ministry of Education, Science, Sports, and Culture, Japan, a fund for "Research for the Future" from the Japan Society for Promotion of Science and a fund for the International Joint Research Grant Program of the New Energy and Industrial Technology Development Organization (NEDO).

References

1 I. Hawkins and A. E. Underhill, *J. Chem. Soc., Chem. Commun.*, 1990, 1593.
2 (*a*) O. A. Dyachenko, S. V. Konovalikhin, A. I. Kotov, G. V. Shilov, E. B. Yagubskii, C. Faulmann and P. Cassoux, *J. Chem. Soc., Chem. Commun.*, 1993, 508; (*b*) S. Schenk, I. Hawkins, S. B. Wilkes, A. E. Underhill and A. Kobayashi, *J. Chem. Soc., Chem. Commun.*, 1993, 1648; (*c*) K. Awaga, T. Okuno, Y. Maruyama, A. Kobayashi, H. Kobayashi, S. Schenk and A. E. Underhill, *Inorg. Chem.*, 1994, **33**, 5598.
3 N. Robertson, K. Awaga, S. Parsons, A. Kobayashi and A. E. Underhill, *Adv. Mater. Opt. Electron.*, 1998, **8**, 93.
4 H. Yamochi, T. Komatsu, N. Matsukawa, G. Saito, T. Mori, M. Kusunoki and K. Sakaguchi, *J. Am. Chem. Soc.*, 1993, **115**, 11319.
5 H. Yamochi, M. Kubota, G. Saito and K. Matsumoto, *Synth. Met.*, 1995, **70**, 1175.
6 Crystan GM6.3, supplied by Mac Science, Japan, 1995.
7 (*a*) T. Mori, A. Kobayashi, H. Kobayashi, G. Saito and H. Inokuchi, *Bull. Chem. Soc. Jpn.*, 1984, **57**, 627; (*b*) R. H. Summerville and R. Hoffmann, *J. Am. Chem. Soc.*, 1976, **98**, 7240

The exponents (ξ) and ionization potentials used in the calculations were taken from ref 7(*a*) for S, C, and H and from ref. 7(*b*) for N and Ni.

8 MOPAC97, Fujitsu Co. Ltd.; J. J. P. Stewart, *J. Comput. Chem.*, 1989, **10**, 209.

9 Although the conductivity of a single crystal was examined, the resistance of the sample exceeded the upper limit of our apparatus ($1 \times 10^9\ \Omega$) due to the small area of the cut end.

10 G. Saito, H. Izukashi, M. Shibata, K. Yoshida, L. A. Kushch, T. Kondo, H. Yamochi, O. O. Drozdova, K. Matsumoto, M. Kusunoki, K. Sakaguchi, N. Kojima and E. B. Yagubskii, *J. Mater. Chem.*, 2000, **10**, 893. In addition to the description in this reference, it should be emphasized that the lowest energy electronic transition of (OMTTF)Br gave a peak at $15.1 \times 10^3\ cm^{-1}$ (662 nm) in CH_3OH solution at room temperature, and even tailing was observed only to $13.0 \times 10^3\ cm^{-1}$ in the lower energy region.

11 Crystal data for $(OMTTF)_2[Ni(tdas)_2]$ at room temperature: $C_{32}H_{32}N_4NiS_{14}$, $M = 980.25$, monoclinic, black plates, $a = 10.160(7)$, $b = 13.851(3)$, $c = 13.678(1)$ Å, $\beta = 96.57(2)^\circ$, $U = 1912(1)$ Å^3, space group $P2_1/a$ (no. 14), $Z = 2$, $\mu(MoK\alpha) = 1.3\ mm^{-1}$, 5657 reflections measured, 1880 unique ($R_{int} = 0.101$), which were used in all the calculations. The final $R(F)$ was 0.055.

12 Although the exact χ_s could not be determined due to the high diamagnetic susceptibility (χ_d) of the core part compared to χ_s (χ_d calculated from Pascal's constant is -3.72×10^{-4} emu per formula unit), the plot of $\chi_s T$ *vs.* T obtained from the static susceptibility measurements by a SQUID magnetometer showed a linear line. This result supports the assignment of the observed EPR signal to a defect of the crystal.

13 When we scanned the potential region from -0.9 to $+1.5$ V (*vs.* SCE), two oxidation peaks were observed at $+0.21$ and 0.81 V without the corresponding reduction peaks in the reverse path (from $+1.5$ to -0.9 V). However, when the scan range was between 0 and $+0.5$ V, the first redox process at $E_{\frac{1}{2}} = 0.18$ V showed a reversible feature. The disappearance of the reduction peaks when the potential is scanned up to too high a value may be the reason for the discrepancy between our result and that reported in ref. 1.

14 G. Saito and J. P. Ferraris, *Bull. Chem. Soc. Jpn.*, 1980, **53**, 2141.

15 J. A. McCleverty, *Prog. Inorg. Chem.*, 1968, **10**, 84.

16 G. Steimecke, H. J. Sieler, R. Kirmse and E. Hoyer, *Phosphorus, Sulfur Relat. Elem.*, 1979, **7**, 49.

17 (*a*) C. T. Vance and R. D. Bereman, *Inorg. Chim. Acta*, 1988, **149**, 229; (*b*) C. T. Vance, J. H. Welch and R. D. Bereman, *Inorg. Chim. Acta*, 1989, **164**, 191.